

## The moving crude adiabatic alternative to the adiabatic representation in excited state dynamics.

R. Maskri<sup>1</sup> and L. Joubert-Doriol<sup>1, a)</sup>

*MSME, Univ Gustave Eiffel, CNRS UMR 8208, Univ Paris Est Creteil,  
F-77474 Marne-la-Vallée, France*

(Dated: 3 May 2022)

The choice of the electronic representation in on-the-fly quantum dynamics is crucial. The adiabatic representation is appealing since adiabatic states are readily available from quantum chemistry packages. The nuclear wavepackets are then expanded in a basis of Gaussian functions, which follow trajectories to explore the potential energy surfaces and approximate the potential using a local expansion of the adiabatic quantities. Nevertheless, the adiabatic representation is plagued with severe limitations when conical intersections are involved: the diagonal Born-Oppenheimer corrections (DBOCs) are non-integrable, and the geometric phase effect on the nuclear wavepackets cannot be accounted for unless a model is available. To circumvent these difficulties, the moving crude adiabatic (MCA) representation was proposed and successfully tested in low energy dynamics where the wavepacket skirts the conical intersection. We assess the MCA representation in the case of non-adiabatic transitions through conical intersections. First, we show that using a Gaussian basis in the adiabatic representation indeed exhibits the aforementioned difficulties with a special emphasis on the possibility to regularize the DBOC terms. Then, we show that MCA is indeed able to properly model non-adiabatic transitions. Tests are done on linear vibronic coupling models for the bis(methylene) adamantyl cation and the butatriene cation.

---

<sup>a)</sup>Electronic mail: [loic.joubert-doriol@univ-eiffel.fr](mailto:loic.joubert-doriol@univ-eiffel.fr)

## I. INTRODUCTION

The Born-Oppenheimer approximation is a cornerstone of chemistry that greatly simplifies the analysis of molecular systems by defining electronic adiabatic states and confining the system in one of these states. Nevertheless, this approximation regularly fails in describing photochemistry, particularly in regions of the potential energy surfaces where the adiabatic states become degenerate and form the commonly encountered conical intersections (CIs)<sup>1,2</sup>. Indeed, the non-adiabatic couplings that are neglected in the Born-Oppenheimer approximation can become arbitrarily large close to a CI<sup>2-4</sup> and break the Born-Oppenheimer approximation. In this case one may believe that including the missing couplings should be sufficient to recover the exact description, but this is not completely true. A first difficulty comes from the fact that the non-adiabatic couplings diverge at the CIs. Hence, all the non-adiabatic coupling terms may not be integrable over the chosen basis and can lead to numerical instabilities. Another difficulty is that an extra geometric phase (GP) attached to the adiabatic states appears upon encircling the CIs<sup>5-8</sup>. The GP implies that adiabatic states have a double-valued boundary condition when revolving around the CI, and so must be the boundary condition on the nuclear wavepackets in order to recover a single valued total molecular wavefunction<sup>6,9</sup>. Overlooking this GP was found to severely impact the resulting dynamics<sup>10-14</sup>. Not accounting for GP diminishes the transition probability in internal conversion processes<sup>15,16</sup>. Even in a low energy regime, when the nuclear wavepacket encircles but does not necessarily have enough energy to reach the CI, the extra GP-induced interference causes appearance of a nodal plane in the nuclear wavepacket<sup>11,17,18</sup> that can diminish population transfer around a CI or even localize the wavepacket on one side of the CI<sup>12,18-20</sup>.

Non-adiabatic dynamics is often described using quantum-classical methods, such as surface hopping<sup>21</sup> or using the exact factorization approach<sup>22</sup>. Regions containing CIs are known to exhibit strong quantum effects due to the strong electron-nuclear couplings, for instance the aforementioned GP-induced interference<sup>11,18,19</sup>. A full quantum approach is then necessary to properly account for these quantum effects. Usual approaches for such simulations use a multiconfiguration expansion in combination with multidimensional grids (see for example the multi configuration time dependent Hartree (MCTDH) method<sup>23,24</sup>). Some drawback of these methods are the necessity of generating a model Hamiltonian be-

forehand, and the fact that grid-based methods scale exponentially with the number of dimensions. Both limitations can be addressed using another common representation of the nuclear wavepackets employing an expansion in terms of time-dependent Gaussian functions<sup>25-33</sup>. This representation has the strong advantage that it avoids evaluation of the Hamiltonian integrals over multidimensional grid by using Gaussian integration when possible, or by utilizing a local approximation motivated by the fact that Gaussian functions have a limited spatial extension. This approach is particularly useful for on-the-fly simulation of molecular systems for which the potential energy surfaces are not known analytically (see for instance the integrals' approximations described in Refs. 34-36). However, a severe drawback of the Gaussian expansion is that Gaussian functions are not double-valued functions. A general approach to solve this difficulty is to remove the GP from the adiabatic states by using an extra phase factor<sup>6</sup>. Nevertheless, choosing the right phase factor requires prior knowledge of the CIs locations. However, their locations are generally not known in on-the-fly simulations of real molecular systems. Thus, it is not always possible to cancel the GP of the adiabatic states<sup>37</sup>. Another drawback comes from the fact that the diagonal elements of the non-adiabatic coupling matrix, also known as diagonal Born-Oppenheimer corrections (DBOCs), are not often calculated in electronic structure packages and are furthermore non-integrable unless special basis functions are utilized<sup>38,39</sup>. Thus, DBOCs are also often overlooked. Despite these difficulties, time-dependent Gaussian functions are very often employed in non-adiabatic dynamics for the advantages they provide in on-the-fly quantum dynamics.

The difficulties appearing at CIs can in principle be resolved by applying a diabaticization of the electronic states<sup>40</sup>. However, only approximate quasi-diabatization are possible<sup>32,36,41,42</sup>, which introduce an additional source of error. Here, we focus on an alternative representation of the electronic states: the moving crude adiabatic (MCA) representation<sup>43-45</sup>. In the MCA representation, the electronic states are solution of the electronic time-independent Schrödinger equation only at the Gaussians' center. Such electronic states do not depend on the nuclear coordinates anymore but rather on the Gaussians' center that are simply time-dependent parameters. Consequently, these states are time-dependent diabatic states, and they do not exhibit GP by construction (they are single-valued, as opposed to the adiabatic states). Hence, the nuclear components are also single-valued, and the single-valuedness of the Gaussian basis functions does not pose any problem (in opposition to the adiabatic case).

Using MCA states was found to properly account for GP effects in low energy dynamics in adiabatic representation<sup>44</sup>, where the extra GP-induced interference causes appearance of a nodal plane in the adiabatic nuclear wavepackets<sup>18,44</sup>. On contrary, the MCA states were not yet tested in the regime of non-adiabatic transitions, where GP participates in enhancing interstate population transfer in the adiabatic representation. Furthermore, the MCA states do not produce non-adiabatic couplings, including DBOC, which is also a powerful advantage for the numerical stability of the simulations.

In this paper, we study the ability of the MCA representation to properly describe the non-adiabatic transitions with a special emphasis on the role of GP and DBOC in the adiabatic representation. The role of GP in this context was found to be twofold: i) it ‘compensates for repulsion caused by the DBOC’<sup>15</sup> and thus facilitates the wavefunction to reach the CI region of large non-adiabatic couplings, and ii) ‘it enhances transfer probability for a component of a nuclear wave-packet that corresponds to the zero eigenvalue of the [angular momentum] operator defined with respect to the CI point’<sup>15</sup>. The first effect, compensation of DBOC, was illustrated on the electron transfer dynamics of the bis(methylene) adamantyl cation (BMA), while the second, enhancement of probability transfer, was best illustrated by the dynamics of the butatriene cation. In the spirit of ref. 15, we start by exhibiting that employing double-valued adiabatic states with nuclear components that are single-valued overlooks the GP such that the resulting dynamics can deviate from the exact result. Then, we numerically expose the ability of the MCA representation to describe the exact dynamics well. We employ the Full Multiple Spawning approach to evolve the Gaussian basis functions<sup>46</sup> with classically evolving Gaussian centers<sup>47</sup>.

The rest of the paper is organized as follows. The theory associated to the adiabatic and MCA representations combined with a Gaussian basis for the nuclei is described in Sec. II. The computational details are given in Sec. III. Section IV contains the results and the discussion. The last section, Sec. V, concludes this paper.

## II. THEORY

### A. The general adiabatic approach for Gaussian expansions

The adiabatic representation is defined by its set of electronic adiabatic states  $\{|\varphi_s(\mathbf{X})\rangle; s = 0, 1, \dots\}$ , which are eigenstates of the electronic Hamiltonian  $\hat{H}_e(\mathbf{X})$ :

$$\hat{H}_e(\mathbf{X}) |\varphi_s(\mathbf{X})\rangle = \varepsilon_s(\mathbf{X}) |\varphi_s(\mathbf{X})\rangle, \quad (1)$$

where  $\{\varepsilon_s(\mathbf{X})\}$  are the adiabatic potential energy surfaces. Here  $\mathbf{x}$  represents the mass-weighted nuclear coordinates and the hat indicates an abstract operator in the Hilbert space of the electrons. Projecting the molecular wavefunction  $|\Psi(\mathbf{X}, t)\rangle$  on this basis gives the Born-Oppenheimer expansion<sup>48</sup>, which is the starting point of many applications in chemistry:

$$|\Psi(\mathbf{X}, t)\rangle = \sum_s |\varphi_s(\mathbf{X})\rangle \chi_s(\mathbf{X}, t), \quad (2)$$

where  $\chi_s(\mathbf{X}, t)$  is the nuclear wavepacket that evolves on the  $s^{\text{th}}$  electronic adiabatic state. In the rest of the paper, we assume atomic units and, unless stated otherwise, we drop the nuclear coordinate dependence for the sake of clarity.

The nuclear component are then obtained as a solution of the time-dependent Schrödinger with the Hamiltonian given by<sup>48</sup>

$$H_{ss'}^{DV} = \left[ -\frac{1}{2} \nabla^t \nabla + \varepsilon_s \right] \delta_{ss'} - \frac{1}{2} \left[ \boldsymbol{\tau}_{ss'}^t \nabla + \nabla^t \boldsymbol{\tau}_{ss'} + \sum_r \boldsymbol{\tau}_{sr}^t \boldsymbol{\tau}_{rs'} \right]. \quad (3)$$

where  $\nabla$  is the gradient associated to the mass-weighted nuclear coordinates,  $\boldsymbol{\tau}_{ss'} = \langle \varphi_s | \nabla \varphi_{s'} \rangle$  is the non-adiabatic coupling vector, and we used bold face letters for vectors and matrices with the superscript 't' to indicate transposition. For the numerical solution, we expand  $\chi_s(t)$  as a linear combination of  $N_s$  Gaussian functions  $\{g(\mathbf{X}; \mathbf{Q}_{sk}(t), \mathbf{P}_{sk}(t)); k = 1, \dots, N_s\}$  on state  $s$  where  $\mathbf{Q}_{sk}(t)$  and  $\mathbf{P}_{sk}(t)$  are time-dependent parameters encoding the centers and the momenta of the Gaussians respectively. The total wavefunction should now read

$$|\Psi(t)\rangle = \sum_s \sum_k^{N_s} C_{sk}(t) |\varphi_s\rangle g(\mathbf{Q}_{sk}(t), \mathbf{P}_{sk}(t)), \quad (4)$$

where  $\{C_{sk}(t)\}$  are expansion coefficients that depend only on time. However, for molecules in vacuum, the electronic Hamiltonian is real, and the adiabatic states are generally chosen to

be real too. In this case, adiabatic electronic states acquire a GP when encircling CIs, which makes them double-valued with respect to revolving around CIs in the nuclear coordinates space. Since the molecular wavefunction is single-valued, it is clear from Eq. 2 that, if  $|\varphi_s\rangle$  has double-valued boundary conditions, then the nuclear components are double-valued too since  $\chi_s(t) = \langle \varphi_s | \Psi(t) \rangle$ . But linear combination using Gaussian functions cannot exhibit these double-valued boundary conditions, because Gaussian functions are single-valued by construction. One way around this difficulty is to compensate the double-valuedness by attaching a double-valued phase factor  $e^{i\alpha_s}$  that depends only on  $\mathbf{X}$  to the adiabatic nuclear components<sup>6</sup>. Then,  $e^{-i\alpha_s}\chi_s(t)$  is also single-valued and can be expanded using Gaussian functions. With this transformation, the molecular Hamiltonian for these single-valued nuclear components takes the following form

$$\begin{aligned}
H_{ss'}^{SV} &= e^{-i\alpha_s} H_{ss'}^{DV} e^{i\alpha_{s'}} \\
&= \left[ -\frac{1}{2} \nabla^t \nabla + \varepsilon_s \right] \delta_{ss'} - \frac{1}{2} \left[ \boldsymbol{\tau}_{ss'}^t \nabla + \nabla^t \boldsymbol{\tau}_{ss'} + \sum_r \boldsymbol{\tau}_{sr}^t \boldsymbol{\tau}_{rs'} \right] e^{i(\alpha_{s'} - \alpha_s)} \\
&\quad - \frac{1}{2} \left[ \mathbf{v}_s^t \mathbf{v}_s + \nabla^t \mathbf{v}_s + \mathbf{v}_s^t \nabla \right] \delta_{ss'} - \frac{1}{2} \left[ \boldsymbol{\tau}_{ss'}^t \mathbf{v}_{s'} + \mathbf{v}_s^t \boldsymbol{\tau}_{ss'} \right] e^{i(\alpha_{s'} - \alpha_s)}, \quad (5)
\end{aligned}$$

where  $\mathbf{v}_s = (i\nabla\alpha_s)$ . This Hamiltonian can be compared to the more familiar one in the double-valued real adiabatic basis,  $\mathbf{H}^{DV}$ , where all phases  $\{\alpha_s\}$  can be considered constant and equal. Unfortunately, the functional form of the phases  $\{\alpha_s\}$  is not generally known for real systems. In this case, the double-valuedness of the nuclear components  $\chi_s$  is often overlooked and  $\mathbf{H}^{DV}$  is utilized even if the nuclear wavepackets are expanded on a Gaussian basis.

The second difficulty comes from the DBOC-related term  $\boldsymbol{\tau}_{sr}^t \boldsymbol{\tau}_{rs}$  when the states  $r$  and  $s$  are degenerate. These terms can be expressed as

$$\boldsymbol{\tau}_{sr}^t \boldsymbol{\tau}_{rs} = -\frac{|\langle \varphi_s | \nabla \hat{H}_e | \varphi_r \rangle|^2}{(\varepsilon_r - \varepsilon_s)^2}, \quad (6)$$

which shows that they become singular at CIs. These singularities are known to be non-integrable for basis functions having non-zero populations at CIs<sup>38</sup>. This non-integrability can be shown for Gaussian functions using a local expansion of the molecular Hamiltonian in the vicinity of a CI. Indeed, when the problematic terms are integrated with Gaussian functions over the full nuclear coordinate space, they give rise to a logarithmic divergence as exposed in App. V. To allow for integration, we add a regularization parameter by sub-

stituting the square of the energy difference  $(\varepsilon_r - \varepsilon_s)^2$  by  $(\varepsilon_r - \varepsilon_s)^2 + \eta$  where  $\eta$  is a small real positive number (see App. V for more details).

## B. The moving crude adiabatic representation

The situation is different in the MCA representation. The electronic states are no more adiabatic but instead solve the electronic Schrödinger equation only at one nuclear geometry, which is chosen to be the centers of the Gaussian functions  $\{\mathbf{Q}_{sk}(t)\}$ :

$$\hat{H}_e(\mathbf{Q}_{sk}(t))|\varphi_s(\mathbf{Q}_{sk}(t))\rangle = \varepsilon_s(\mathbf{Q}_{sk}(t))|\varphi_s(\mathbf{Q}_{sk}(t))\rangle. \quad (7)$$

The molecular wavefunction now reads

$$|\Psi(t)\rangle = \sum_s \sum_k^{N_s} C_{sk}(t) |\varphi_s(\mathbf{Q}_{sk}(t))\rangle g(\mathbf{Q}_{sk}(t), \mathbf{P}_{sk}(t)), \quad (8)$$

and the molecular Hamiltonian

$$H_{ss',kl}^{MCA} = -\frac{1}{2} \langle \varphi_s(\mathbf{Q}_{sk}(t)) | \varphi_{s'}(\mathbf{Q}_{s'l}(t)) \rangle \nabla^t \nabla + \left\langle \varphi_s(\mathbf{Q}_{sk}(t)) \left| \hat{H}_e \right| \varphi_{s'}(\mathbf{Q}_{s'l}(t)) \right\rangle. \quad (9)$$

This last Hamiltonian is different from the Hamiltonians using adiabatic states (Eqs. (5-6)) in the sense there are no non-adiabatic couplings  $\boldsymbol{\tau}_{ss'}$  involved. This is due to the fact that MCA states do not depend on the nuclear coordinates and are therefore strictly diabatic. Therefore, there are no terms in the Hamiltonian that are non-integrable with a Gaussian basis. Another strong advantage is that, since the MCA states do not depend on the nuclear coordinates, they are single-valued in the nuclear coordinates space by construction. Hence, Gaussian functions can be employed for the expansion of the nuclear wavepackets.

## III. COMPUTATIONAL DETAILS

### A. Hamiltonian models

We utilize 2-dimensional 2-state linear vibronic coupling models to simulate the electron transfers in BMA and in the butatriene cation. The general form of the model is given in the diabatic representation and in mass and frequency weighted coordinates

$$\mathbf{H}^{dia} = -\frac{1}{2} \nabla^t \boldsymbol{\omega} \nabla \begin{pmatrix} 1 & 0 \\ 0 & 1 \end{pmatrix} + \mathbf{H}_e, \quad (10)$$

$$\mathbf{H}_e = \frac{1}{2} \left[ (\mathbf{X}^t \boldsymbol{\omega} \mathbf{X} + \mathbf{X}^t \boldsymbol{\sigma} + \epsilon_\sigma) \begin{pmatrix} 1 & 0 \\ 0 & 1 \end{pmatrix} + (\mathbf{X}^t \boldsymbol{\kappa} + \epsilon_\kappa) \begin{pmatrix} -1 & 0 \\ 0 & 1 \end{pmatrix} + (\mathbf{X}^t \boldsymbol{\lambda} + \epsilon_\lambda) \begin{pmatrix} 0 & 1 \\ 1 & 0 \end{pmatrix} \right]. \quad (11)$$

The models are obtained from Ref. 15, and originally from Refs. 49,50, after transformation to mass and frequency weighted coordinates. The parameters are given in Tab. I

TABLE I. Parameters for the two molecular systems in atomic units. Parameters come from Ref. 15 after transformation to mass and frequency weighted coordinates.

System	$\omega_{11}$	$\omega_{22}$	$\sigma_1$	$\kappa_1$	$\lambda_2$	$\epsilon_\kappa$
$\text{C}_4\text{H}_4^+$	$9.56 \cdot 10^{-3}$	$3.35 \cdot 10^{-3}$	$-1.88 \cdot 10^{-2}$	$1.88 \cdot 10^{-2}$	$2.12 \cdot 10^{-2}$	$1.45 \cdot 10^{-3}$
BMA	$7.74 \cdot 10^{-3}$	$6.68 \cdot 10^{-3}$	0.00	$-2.126 \cdot 10^{-2}$	$9.90 \cdot 10^{-4}$	0.00
For both systems $\omega_{12} = \omega_{21} = 0$ , $\sigma_2 = \kappa_2 = \lambda_1 = 0$ , $\epsilon_\lambda = \epsilon_\sigma = 0$						

## B. The Gaussian basis

The Gaussian basis is chosen as frozen-width coherent states with the form

$$g(\mathbf{Q}_{sk}(t), \mathbf{P}_{sk}(t)) = \exp\left(-\frac{1}{2}\mathbf{X}^t\mathbf{X} + \mathbf{X}^t\mathbf{b}_{sk}(t) + c_{sk}(t)\right), \quad (12)$$

where

$$\mathbf{b}_{sk}(t) = \mathbf{Q}_{sk}(t) + i\mathbf{P}_{sk}(t), \quad (13)$$

$$c_{sk}(t) = -\frac{1}{2}\mathbf{Q}_{sk}^t(t)\mathbf{b}_{sk}(t) - \frac{\mathcal{D}\log(\pi)}{4}, \quad (14)$$

and  $\mathcal{D}$  is the dimensionality of the system.

The time evolution of the parameters is dictated by classical equations of motion on the corresponding adiabatic surfaces:

$$\dot{\mathbf{Q}}_{sk}(t) = \boldsymbol{\omega}\mathbf{P}_{sk}(t), \quad (15)$$

$$\dot{\mathbf{P}}_{sk}(t) = -\frac{1}{2}\left(2\boldsymbol{\omega}\mathbf{Q}_{sk}(t) + \boldsymbol{\sigma} \pm \frac{\boldsymbol{\kappa}(\mathbf{Q}_{sk}^t(t)\boldsymbol{\kappa} + \epsilon_\kappa) + \boldsymbol{\lambda}(\mathbf{Q}_{sk}^t(t)\boldsymbol{\lambda} + \epsilon_\lambda)}{\sqrt{(\mathbf{Q}_{sk}^t(t)\boldsymbol{\kappa} + \epsilon_\kappa)^2 + (\mathbf{Q}_{sk}^t(t)\boldsymbol{\lambda} + \epsilon_\lambda)^2}}\right), \quad (16)$$

where the plus (minus) sign is associated to the upper (lower) adiabatic state.

The spawning procedure follows the prescription of Ref. 46. The technical details of this spawning procedure as well as the integration scheme for equations of motion and the integration over the Gaussian basis of the Hamiltonian is described in the supplementary material<sup>51</sup>. Gaussian-based calculations are compared to exact calculations using a finite basis representation of the Hamiltonians in Eqs. (10-11), which is also described in the supplementary material<sup>51</sup>. All simulations are done with the Octave package<sup>52</sup>.



## IV. RESULTS AND DISCUSSION

We test the methods on the internal conversion process. The initial state is depicted by a single Gaussian basis function placed on the upper electronic state at positions (0.632, 0) for the butatriene cation and (-1.366, 0) for BMA with zero momentum in both cases. We then generate other unpopulated Gaussians according to this initial Gaussian distribution with symmetric sampling. The starting number of Gaussian functions  $N_i$  is given in Tab. II. Along the dynamics, new spawned Gaussian basis functions increase this number to a final one  $N_f$ . We start by testing the simulations in adiabatic representation, and then test the MCA representation. These tests are done by comparing the adiabatic populations with respect to the exact simulations.

TABLE II. Initial and final number of basis functions used in the Gaussian-based simulations for both models in adiabatic and MCA representations.

	BMA	C <sub>4</sub> H <sub>4</sub> <sup>+</sup>
Adiabatic	$N_i = 256; N_f = 328$	$N_i = 346; N_f = 416$
MCA	$N_i = 251; N_f = 326$	$N_i = 339; N_f = 442$

### A. Adiabatic simulations

We follow the adiabatic population obtained using a Gaussian basis in combination with the double-valued electronic states. This is equivalent to employ the Hamiltonian given in Eq. 6 but overlooking the GP since the Gaussian basis is single valued.

We first test the impact of DBOC in the dynamics of BMA where it plays an important role due to the small diabatic coupling<sup>15</sup>. In this case, DBOC plays the role of an infinite potential at the CI that prevents the nuclear wavepackets to access the region of strong non-adiabatic couplings and thus diminishes the non-adiabatic transitions. This effect is however counterbalanced by a similar term generated by the GP such that the wavepackets can approach the CI, which allow for larger non-adiabatic transitions. Hence, a calculation that properly includes the DBOC term without GP must show a decrease in the population transfer as observed in Ref. 15. This will be our test to assess the proper account for DBOC. Since, the DBOC terms,  $\tau_{ss'}^t \tau_{s's}$ , are non-integrable, we employ a regularized version of these

terms as depicted at the end of Sec. II-II A (and also developed in App. V) with various values of  $\eta$ . Results are given in Fig. 1. They show that for large values of  $\eta$ , the repelling effect of DBOC is significantly reduced and does not play a significant role. However, for small values,  $\eta = 10^{-9}, 10^{-12}$ , DBOC clearly diminishes the population transfer in agreement with Ref. 15. We deduce that if  $\eta$  is sufficiently small, the regularized DBOC can reproduce the effect of the exact DBOC. We then test the compensation of GP and DBOC: it was previously found that when GP is not included in the simulation, not including DBOC improves the results<sup>15</sup>. This is indeed what we observe in Fig. 1 for the ‘no DBOC’ case, where the initial population dynamics is captured when both GP and DBOC are overlooked.

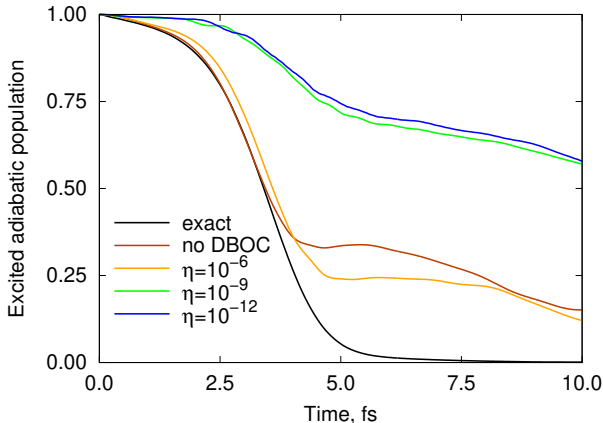


FIG. 1. Comparison between adiabatic simulation without GP for various values of the regularization parameter  $\eta$ , for BMA.

We now test the impact of GP in enhancing the transfer probability for the components of the wavepackets with zero angular momentum with respect to the CI<sup>15</sup>. This effect is better illustrated in the case of the butatriene cation, where the wavepacket has a large component (87%) with zero angular momentum when arriving at the CI<sup>15</sup>. Figure 2-a) shows that DBOC only has a minor impact on the population evolution. Indeed, including DBOC or not, does not significantly affect the population dynamics. This absence of effect also appears through the fact that the value of the regularization parameter does not significantly change the results. To expose the GP effect associated to enhancing probability transfer, the component of the wavepacket that is associated to a zero expectation value of the angular momentum is artificially reduced by changing the initial state as in Ref. 15. We use an initial state defined as a linear combination of two Gaussians centered at  $(-1.366, \pm 2.8 \cdot 10^{-3})$

with coefficients of opposite signs  $C_1(0) = 1 = -C_2(0)$ . This initial state reproduces the original single-Gaussian state multiplied by  $X_2$ , which creates a nodal line  $X_2 = 0$  in the wave-packet and eliminates the component associated to a zero expectation value of the angular momentum. The result, given in Fig. 2-b), clearly shows that employing this new initial condition reduces the difference between the exact population dynamics and the one obtained in the Gaussian basis (without GP). Consequently, the Gaussian-based method now captures the non-adiabatic transition.

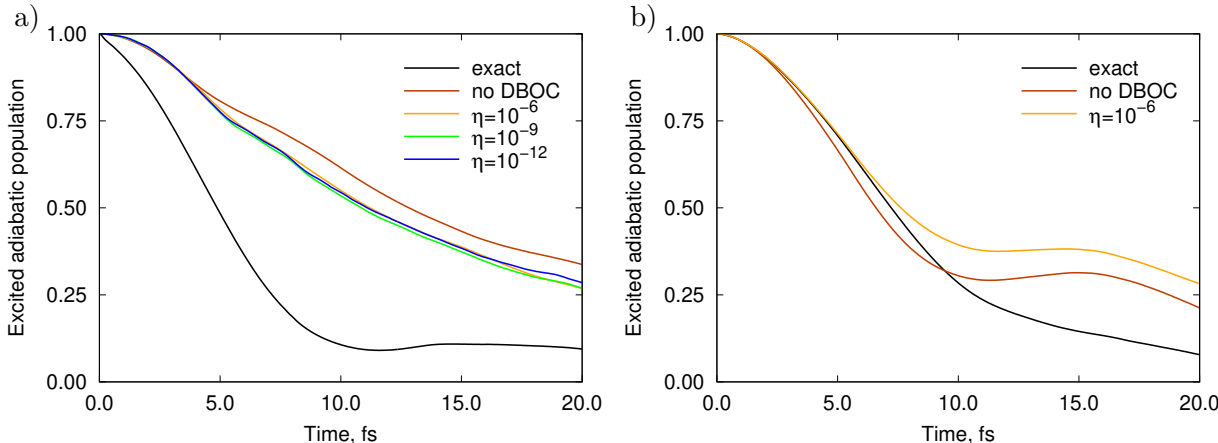


FIG. 2. Comparison between adiabatic simulations without GP for various values of the regularization parameter  $\eta$ , for the butatriene cation. Initial conditions are taken as: a) one Gaussian function centered at  $(-1.366, 0)$ , and b) two Gaussian functions at  $(-1.366, \pm 2.8 \cdot 10^{-3})$  with opposite coefficients, on the upper adiabatic state in both cases.

We observe that integration of DBOC can be mimicked with a right choice of the regularization parameter  $\eta$ . Hence, non-integrability of DBOC appears to be less problematic than expected for the models studied in this article. We also observed that all the results in adiabatic representation agree with the previously reported simulations using the same models<sup>15</sup>, which are not including the GP. This numerical argument shows that GP is not included when using a Gaussian basis with the Hamiltonian given by Eq. 6.

## B. MCA simulations

In this case, the initial state population is not fully on the upper adiabatic state because the MCA electronic states are not adiabatic. Indeed, creating an initial state that is strictly

on the upper adiabatic state would require a linear combination of MCA states whose positions are optimized to maximize overlap with the initial Gaussian state in the adiabatic representation. However, such a construction is not necessary because we are interested in showing that dynamics in the MCA states converges to the exact dynamics independently from the initial conditions. The adiabatic population can still be calculated from the MCA calculations by using the scheme explained in the supplementary material<sup>51</sup>. For BMA, the initial populated Gaussian is far enough from the CI and the diabatic coupling is small enough so that the initial upper state population is close to 1. However, for the butatriene cation, the initial upper population is closer to 0.75. We model this same initial states in the exact calculations as well. The upper state adiabatic population is then calculated using the Gaussian integration technique described in the supplementary material<sup>51</sup>. The comparison between the exact population evolution and the dynamics obtained using the MCA representation is given in Fig. 3. These results show that the MCA representation reproduces the exact probability transfer.

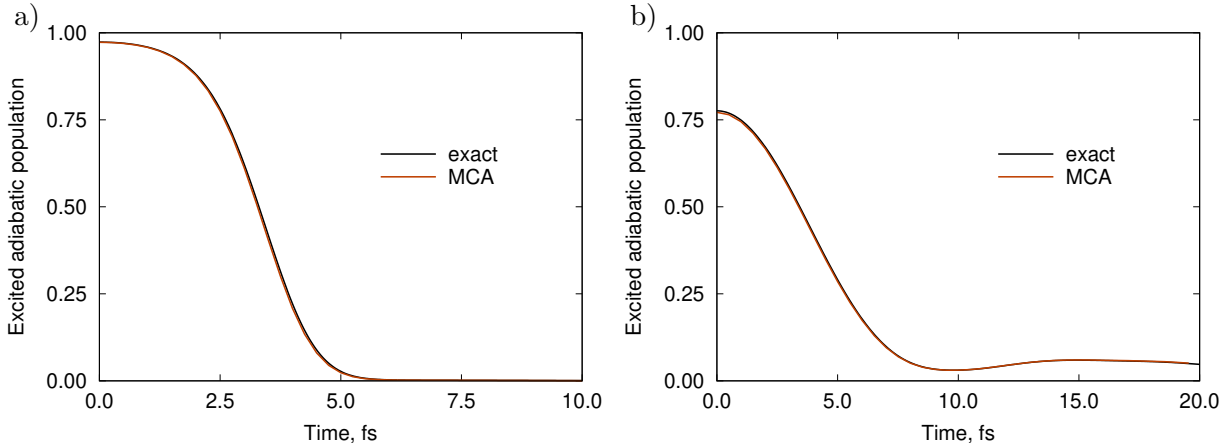


FIG. 3. Comparison between the upper adiabatic state time-dependent population using the MCA representation and the exact calculation for: a) BMA and b) C<sub>4</sub>H<sub>4</sub><sup>+</sup>.

We test the convergence by comparing the autocorrelation functions  $|\langle \Psi(0) | \Psi(t) \rangle|$  for these dynamics after extracting the spectra calculated by Fourier transform of these autocorrelation functions. These spectra, given in Fig. 4, show perfect agreement between the spectra obtain with the exact calculation and the one using the MCA representation.

Both the adiabatic population evolution and the Fourier transform of the autocorrelation function agree to show that the MCA representation can be used to generate the exact

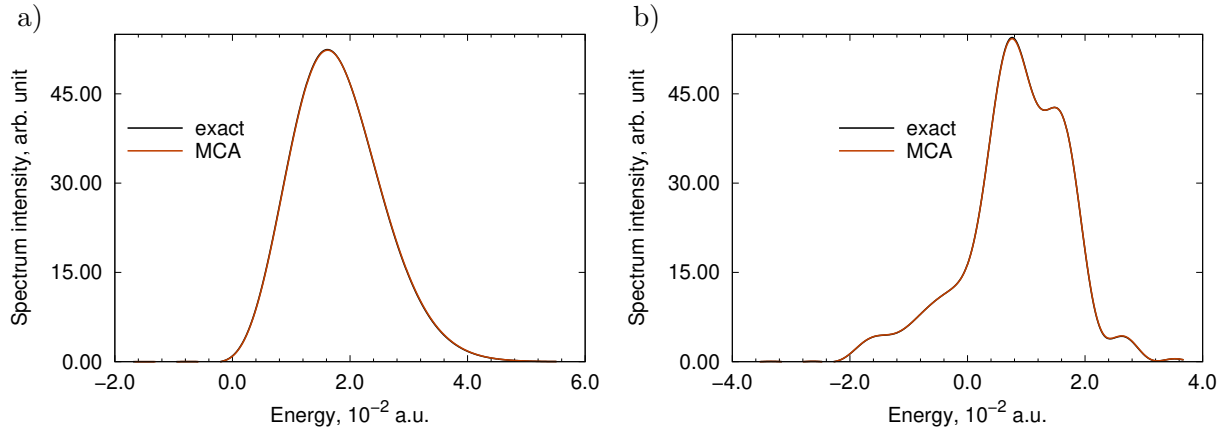


FIG. 4. Comparison between the spectra obtained using the MCA representation and the exact calculation for: a) BMA and b)  $C_4H_4^+$ .

dynamics.

## V. CONCLUSION

In this paper, we assess the ability of Gaussian-based methods to reproduce the exact dynamics while employing adiabatic electronic states.

We observed that using Gaussian functions in the adiabatic representation exhibits the same problems as in Ref. 15: not including GP results in time evolutions that deviate from the exact solution. Therefore, we can conclude that using Gaussian functions fails in properly accounting GP, and one must be cautious when the dynamics involve CIs.

We also studied the problem of the non-integrability of DBOC in the adiabatic representation. As expected from Ref. 38, we found that this term is indeed non-integrable in a Gaussian basis. Nevertheless, we applied a regularization that makes the integral calculation possible thanks to an extra small parameter in the denominator. We observed that for small enough values of this parameter, the dynamics behaves similarly to what was observed in Ref. 15. Hence, non-integrability of DBOC is not a major problem for the dynamical processes that are studied here.

Finally, we tested the dynamics obtained using the MCA representation. We found that this representation can properly reproduce the exact time evolution of the adiabatic population, and also the autocorrelation function. Thus, we can conclude that the MCA

representation is capable of describing correctly internal conversion processes.

These numerical evidences of MCA validity are important since this representation still employs the adiabatic states (at the Gaussians' center) obtained from quantum chemistry packages, but with the strong advantage that it does not need any integral regularization or extra phase factor. Furthermore, the MCA representation also has the advantage that it alleviates the need to potential energy models by applying Gaussian integration techniques on the exact molecular Hamiltonian<sup>45</sup>. Hence, validating MCA in the context of non-adiabatic transitions is an important step before further developments related to the exact integration of the molecular Hamiltonian.

## ACKNOWLEDGEMENTS

LJD and RM are grateful to Michael Schuurman for fruitful discussions on the implementation of the full multiple spawning algorithm, and Artur Izmaylov, Mina Asaad, and Alexander Mitrushchenkov for their comments on the manuscript. This work was supported by the 2021 Mobility and International Cooperation Incentive Call of the I-SITE FUTURE.

## EXPOSITION AND REGULARIZATION OF THE DIVERGING TERM IN DBOC

In this appendix, we derive an expression of the DBOC integrated over Gaussian basis functions for the models of the form given in Eq. 10. The non-adiabatic coupling vector takes the form

$$\boldsymbol{\tau}_{12} = \frac{1}{2} \frac{\boldsymbol{\kappa}(\mathbf{X}^t \boldsymbol{\lambda} + \epsilon_\lambda) - \boldsymbol{\lambda}(\mathbf{X}^t \boldsymbol{\kappa} + \epsilon_\kappa)}{(\mathbf{X}^t \boldsymbol{\kappa} + \epsilon_\kappa)^2 + (\mathbf{X}^t \boldsymbol{\lambda} + \epsilon_\lambda)^2}. \quad (17)$$

For further simplification of the expressions, we operate a translation to place the CI's position  $\mathbf{X}_{CI}$  in the center of the new coordinate system  $\tilde{\mathbf{X}} = \mathbf{X} - \mathbf{X}_{CI}$ . The CI's position is obtained by minimizing the energy under the constraints  $\mathbf{X}^t \boldsymbol{\kappa} + \epsilon_\kappa = \mathbf{X}^t \boldsymbol{\lambda} + \epsilon_\lambda = 0$ :

$$\begin{aligned} \mathbf{X}_{CI} = & -\frac{1}{2} \boldsymbol{\omega}^{-1} \left( \boldsymbol{\omega} - (\boldsymbol{\kappa} \boldsymbol{\lambda}) [(\boldsymbol{\kappa} \boldsymbol{\lambda})^t \boldsymbol{\omega}^{-1} (\boldsymbol{\kappa} \boldsymbol{\lambda})]^{-1} (\boldsymbol{\kappa} \boldsymbol{\lambda})^t \right) \boldsymbol{\omega}^{-1} \boldsymbol{\sigma} \\ & - \boldsymbol{\omega}^{-1} (\boldsymbol{\kappa} \boldsymbol{\lambda}) [(\boldsymbol{\kappa} \boldsymbol{\lambda})^t \boldsymbol{\omega}^{-1} (\boldsymbol{\kappa} \boldsymbol{\lambda})]^{-1} \begin{pmatrix} \epsilon_\kappa \\ \epsilon_\lambda \end{pmatrix}. \end{aligned} \quad (18)$$

Furthermore, we rotate the coordinates to diagonalize the matrix  $\boldsymbol{\kappa} \boldsymbol{\kappa}^t + \boldsymbol{\lambda} \boldsymbol{\lambda}^t$ , using the rotation  $\mathbf{R}$  so that  $\bar{\mathbf{X}} = \mathbf{R}^t \tilde{\mathbf{X}}$  and  $\mathbf{R}^t (\boldsymbol{\kappa} \boldsymbol{\kappa}^t + \boldsymbol{\lambda} \boldsymbol{\lambda}^t) \mathbf{R} = \bar{\mathbf{g}}$  has only two non-zero eigenvalues

(by construction) that we order as  $\bar{\mathbf{g}} = \text{diag}(\bar{g}_1, \bar{g}_2, 0, \dots)$ . These combined translation and rotation redefine several quantities that we indicate with a bar and that are summarized here:

$$\bar{\mathbf{X}} = \mathbf{R}^t(\mathbf{X} - \mathbf{X}_{CI}), \quad (19)$$

$$\bar{\boldsymbol{\sigma}} = \mathbf{R}^t(\boldsymbol{\sigma} + 2\boldsymbol{\omega}\mathbf{X}_{CI}), \quad (20)$$

$$\bar{\epsilon}_\sigma = \epsilon_\sigma + \mathbf{X}_{CI}^t \boldsymbol{\sigma} + \mathbf{X}_{CI}^t \boldsymbol{\omega} \mathbf{X}_{CI}, \quad (21)$$

$$\bar{\epsilon}_\kappa = \bar{\epsilon}_\lambda = 0, \quad (22)$$

$$\bar{\mathbf{g}} = \mathbf{R}^t(\boldsymbol{\kappa}\boldsymbol{\kappa}^t + \boldsymbol{\lambda}\boldsymbol{\lambda}^t)\mathbf{R}, \quad (23)$$

$$\bar{\mathbf{K}} = -\mathbf{R}^t(\boldsymbol{\kappa}\boldsymbol{\lambda}^t - \boldsymbol{\lambda}\boldsymbol{\kappa}^t)\boldsymbol{\omega}(\boldsymbol{\kappa}\boldsymbol{\lambda}^t - \boldsymbol{\lambda}\boldsymbol{\kappa}^t)\mathbf{R}, \quad (24)$$

$$\bar{\mathbf{b}}_{ss'kl}(t) = \frac{1}{2}\mathbf{R}^t(\mathbf{b}_{sk}^*(t) + \mathbf{b}_{s'l}(t) - 2\mathbf{X}_{CI}), \quad (25)$$

$$\bar{c}_{ss'kl}(t) = c_{sk}^*(t) + \mathbf{X}_{CI}^t \mathbf{b}_{sk}^*(t) + c_{s'l}(t) + \mathbf{X}_{CI}^t \mathbf{b}_{s'l}(t) - \mathbf{X}_{CI}^t \mathbf{X}_{CI}. \quad (26)$$

The DBOC term now takes the form

$$\boldsymbol{\tau}_{12}^t \boldsymbol{\tau}_{21} = \boldsymbol{\tau}_{21}^t \boldsymbol{\tau}_{12} = -\frac{1}{4} \frac{\bar{\mathbf{X}}^t \bar{\mathbf{K}} \bar{\mathbf{X}}}{(\bar{\mathbf{X}}^t \bar{\mathbf{g}} \bar{\mathbf{X}})^2}. \quad (27)$$

Since integration of DBOC is expected to diverge, we integrate a regularized version of the operator by adding a small positive number  $\eta$  in the denominator function. The integrals we need to evaluate now read

$$I = \frac{1}{8} \int_{\mathbb{R}^D} d\tilde{V} \frac{\bar{\mathbf{X}}^t \bar{\mathbf{K}} \bar{\mathbf{X}} e^{-\bar{\mathbf{X}}^t \bar{\mathbf{X}} + 2\bar{\mathbf{X}}^t \bar{\mathbf{b}}_{ss'kl}(t) + \bar{c}_{ss'kl}(t)}}{(\bar{\mathbf{X}}^t \bar{\mathbf{g}} \bar{\mathbf{X}} + \eta)^2}. \quad (28)$$

For the evaluation, we use the definition of the Gamma function to rewrite the denominator as

$$(\bar{\mathbf{X}}^t \bar{\mathbf{g}} \bar{\mathbf{X}} + \eta)^{-2} = 2 \int_0^\infty dr r^3 e^{-r^2(\bar{\mathbf{X}}^t \bar{\mathbf{g}} \bar{\mathbf{X}} + \eta)}. \quad (29)$$

Substituting the denominator in Eq. 28 using the relation Eq. 29, and performing the Gaussian integration, we obtain a one-dimensional integral:

$$I = \frac{S_{ss'kl}(t)}{4} \int_0^\infty dr r^3 e^{-r^2 \eta - r^2 \left( \frac{\bar{b}_{ss'kl,1}^2(t) \bar{g}_1}{1+r^2 \bar{g}_1} + \frac{\bar{b}_{ss'kl,2}^2(t) \bar{g}_2}{1+r^2 \bar{g}_2} \right)} \times \left( \frac{\bar{b}_{ss'kl,1}^2(t) \bar{K}_{11}}{(1+r^2 \bar{g}_1)^2} \right. \\ \left. + 2 \frac{\bar{b}_{ss'kl,1}(t) \bar{b}_{ss'kl,2}(t) \bar{K}_{12}}{(1+r^2 \bar{g}_1)(1+r^2 \bar{g}_2)} + \frac{\bar{b}_{ss'kl,2}^2(t) \bar{K}_{22}}{(1+r^2 \bar{g}_2)^2} + \frac{1}{2} \frac{\bar{K}_{11}}{1+r^2 \bar{g}_1} + \frac{1}{2} \frac{\bar{K}_{22}}{1+r^2 \bar{g}_2} \right), \quad (30)$$

where  $S_{ss'kl}(t) = \pi^{D/2} \exp(\bar{\mathbf{b}}_{ss'kl}^t(t) \bar{\mathbf{b}}_{ss'kl}(t) + \bar{c}_{ss'kl}(t))$  is the Gaussian overlap. This integral can be brought to an integral over a finite range by performing the change of variable  $r^2 = u^2/(1 - u^2\bar{g}_1)$  [ $r^3 dr = u^3 du/(1 - u^2\bar{g}_1)^3$ ] and defining  $\Delta\bar{g} = \bar{g}_1 - \bar{g}_2$ :

$$I = \frac{S_{ss'kl}(t)}{4} \int_0^{\bar{g}_1^{-1/2}} du u^3 \frac{e^{-\frac{u^2\eta}{1-u^2\bar{g}_1} - u^2 \left( \bar{b}_{ss'kl,1}^2(t)\bar{g}_1 + \frac{\bar{b}_{ss'kl,2}^2(t)\bar{g}_2}{1-u^2\Delta\bar{g}} \right)}}{\sqrt{1 - u^2\Delta\bar{g}}} \times \left( \bar{K}_{11} \bar{b}_{ss'kl,1}^2(t) \right. \\ \left. + 2 \frac{\bar{K}_{12} \bar{b}_{ss'kl,1}(t) \bar{b}_{ss'kl,2}(t)}{1 - u^2\Delta\bar{g}} + \frac{\bar{K}_{22} \bar{b}_{ss'kl,2}^2(t)}{(1 - u^2\Delta\bar{g})^2} + \frac{1}{2} \frac{\bar{K}_{11}}{(1 - u^2\bar{g}_1)} + \frac{1}{2} \frac{\bar{K}_{22}}{(1 - u^2\Delta\bar{g})(1 - u^2\bar{g}_1)} \right). \quad (31)$$

The last two terms diverge in the upper limit of the integral. However, we can add and remove these terms in their upper limit to isolate the singularities and analytically integrate them:

$$I = \frac{S_{ss'kl}(t)}{4} \left( \frac{\bar{K}_{11}}{\bar{g}_1} + \frac{\bar{K}_{22}}{\bar{g}_2} \right) \frac{e^{-(\bar{b}_{ss'kl,1}^2(t) + \bar{b}_{ss'kl,2}^2(t))}}{4\sqrt{\bar{g}_1\bar{g}_2}} e^{\frac{\eta}{2\bar{g}_1}} K_0 \left( \frac{\eta}{2\bar{g}_1} \right) \\ + \frac{S_{ss'kl}(t)}{4} \int_0^{\bar{g}_1^{-1/2}} du \left[ u^3 \frac{e^{-\frac{u^2\eta}{1-u^2\bar{g}_1} - u^2 \left( \bar{b}_{ss'kl,1}^2(t)\bar{g}_1 + \frac{\bar{b}_{ss'kl,2}^2(t)\bar{g}_2}{1-u^2\Delta\bar{g}} \right)}}{\sqrt{1 - u^2\Delta\bar{g}}} \times \left( \bar{K}_{11} \bar{b}_{ss'kl,1}^2(t) \right. \right. \\ \left. \left. + 2 \frac{\bar{K}_{12} \bar{b}_{ss'kl,1}(t) \bar{b}_{ss'kl,2}(t)}{1 - u^2\Delta\bar{g}} + \frac{\bar{K}_{22} \bar{b}_{ss'kl,2}^2(t)}{(1 - u^2\Delta\bar{g})^2} + \frac{1}{2} \frac{\bar{K}_{11}}{(1 - u^2\bar{g}_1)} + \frac{1}{2} \frac{\bar{K}_{22}}{(1 - u^2\Delta\bar{g})(1 - u^2\bar{g}_1)} \right) \right. \\ \left. - \left( \frac{\bar{K}_{11}}{\bar{g}_1} + \frac{\bar{K}_{22}}{\bar{g}_2} \right) \frac{e^{-(\bar{b}_{ss'kl,1}^2(t) + \bar{b}_{ss'kl,2}^2(t))}}{2\sqrt{\bar{g}_2}} \frac{e^{-\frac{u^2\eta}{1-u^2\bar{g}_1}}}{1 - u^2\bar{g}_1} \right], \quad (32)$$

where  $K_0$  is the Bessel function of second kind, which has the following expansion using the Euler-Mascheroni constant  $\gamma$

$$K_0 \left( \frac{\eta}{2\bar{g}_1} \right) = \log(8\bar{g}_1) - \log(\eta) - \gamma + \frac{\eta^2}{64\bar{g}_1^2} (\log(8\bar{g}_1) - \log(\eta) - \gamma + 1) + \mathcal{O}(\eta^4). \quad (33)$$

The integral in Eq. 32 now converges to a finite value, and we shall focus on the first term. It is clear that the first term on the right-hand side of Eq. 33,  $\log(8\bar{g}_1/\eta)$ , diverges in the limit where  $\eta \rightarrow 0$ , while the remaining terms have a finite value. Hence, the DBOC term is non-integrable for Gaussian functions in a linear vibronic coupling model and gives rise to a logarithmic divergence as it was found in Ref. 38.

## REFERENCES

- <sup>1</sup>Yarkony DR. 2001 Conical Intersections: The New Conventional Wisdom. *J. Phys. Chem. A* **105**, 6277. See <https://doi.org/10.1021/jp003731u>



- <sup>2</sup>Migani A and Olivucci M. 2004. *Conical Intersections and Organic reaction mechanisms* in *Conical Intersections*, **15**, 271-320. Singapore: World Scientific. See [https://doi.org/10.1142/9789812565464\\_0006](https://doi.org/10.1142/9789812565464_0006)
- <sup>3</sup>Baer M. 2006. *Beyond Born-Oppenheimer: Conical Intersections and Electronic Nonadiabatic Coupling Terms*. John Wiley & Sons Ltd, 26-138. See <https://doi.org/10.1002/0471780081>
- <sup>4</sup>Yarkony DR. 2004. *Conical Intersections: their Description and Consequences* in *Conical Intersections*, **15**, 41-127. Singapore: World Scientific. See [https://doi.org/10.1142/9789812565464\\_0002](https://doi.org/10.1142/9789812565464_0002)
- <sup>5</sup>Berry MV. 1984 Quantal phase factors accompanying adiabatic changes. *Proc. R. Soc. A* **392**, 45. See <https://doi.org/10.1098/rspa.1984.0023>
- <sup>6</sup>Mead CA and Truhlar DG. 1979 On the determination of Born-Oppenheimer nuclear motion wave functions including complications due to conical intersections and identical nuclei. *J. Chem. Phys.* **70**, 2284. See <https://doi.org/10.1063/1.437734>
- <sup>7</sup>Mead C. 1980 The molecular Aharonov-Bohm effect in bound states. *Chem. Phys.* **49**, 23. See [https://doi.org/10.1016/0301-0104\(80\)85035-X](https://doi.org/10.1016/0301-0104(80)85035-X)
- <sup>8</sup>Berry MV. 1987. Quantum phase corrections from adiabatic iteration. *Proc. R. Soc. A* **414**, 31. See <https://doi.org/10.1098/rspa.1987.0131>
- <sup>9</sup>Longuet-Higgins HC, Opik U, Pryce MHL, and Sack RA. 1958 Studies of the Jahn-Teller effect. II. The dynamical problem. *Proc. R. Soc. A* **244**, 1. See <https://doi.org/10.1098/rspa.1958.0022>
- <sup>10</sup>Ryabinkin IG, Joubert-Doriol L, Izmaylov AF. 2017 Geometric Phase Effects in Nonadiabatic Dynamics near Conical Intersections. *Acc. Chem. Res.* **50**, 1785. See <https://doi.org/10.1021/acs.accounts.7b00220>
- <sup>11</sup>Xie C, Ma J, Zhu X, Yarkony DR, Xie D, Guo H. 2016 Nonadiabatic Tunneling in Photodissociation of Phenol. *J. Am. Chem. Soc.* **138**, 7828. See <http://dx.doi.org/10.1021/jacs.6b03288>
- <sup>12</sup>Henshaw S, Izmaylov AF. 2017 Topological Origins of Bound States in the Continuum for Systems with Conical Intersections. *J. Phys. Chem. Lett.* **9**, 146. See <https://doi.org/10.1021/acs.jpcclett.7b02791>
- <sup>13</sup>Neville SP, Stolow A, Schuurman MS. 202 The role of geometric phase in the formation of electronic coherences at conical intersections. arXiv:2011.06728 [physics.chem-ph]. See

<https://arxiv.org/abs/2011.06728>

- <sup>14</sup>Xie C, Malbon CL, Guo H, Yarkony DR. 2019 Up to a Sign. The Insidious Effects of Energetically Inaccessible Conical Intersections on Unimolecular Reactions. *Acc. Chem. Res.* **52**, 501. See <https://doi.org/10.1021/acs.accounts.8b00571>
- <sup>15</sup>Ryabinkin IG, Joubert-Doriol L, Izmaylov AF. 2014 When Do We Need to Account for the Geometric Phase in Excited State Dynamics? *J. Chem. Phys.* **140**, 214116. See <https://doi.org/10.1063/1.4881147>
- <sup>16</sup>Li J, Joubert-Doriol L, Izmaylov AF. 2017 Geometric phase effects in excited state dynamics through a conical intersection in large molecules: N-dimensional linear vibronic coupling model study. *J. Chem. Phys.* **147**, 064106. See <https://doi.org/10.1063/1.4985925>
- <sup>17</sup>Schön J, Köppel, H. 1995 Geometric Phase Effects and Wave Packet Dynamics on Intersecting Potential Energy Surfaces. *J. Chem. Phys.* **103**, 9292. See <http://dx.doi.org/10.1063/1.469988>
- <sup>18</sup>Ryabinkin IG, Izmaylov AF. 2013 Geometric Phase Effects in Dynamics Near Conical Intersections: Symmetry Breaking and Spatial Localization. *Phys. Rev. Lett.* **111**, 220406. See <https://doi.org/10.1103/physrevlett.111.220406>
- <sup>19</sup>Joubert-Doriol L, Ryabinkin IG, Izmaylov AF. 2013 Geometric Phase Effects in Low-Energy Dynamics Near Conical Intersections: A Study of the Multidimensional Linear Vibronic Coupling Model. *J. Chem. Phys.* **139**, 234103. See <https://doi.org/10.1063/1.4844095>
- <sup>20</sup>Joubert-Doriol L, Izmaylov AF. 2017 Molecular “topological insulators”: a case study of electron transfer in the bis (methylene) adamantyl carbocation. *Chem. Commun.* **53**, 7365. See <http://dx.doi.org/10.1039/C7CC02275A>
- <sup>21</sup>Tully JC. 1998 Mixed quantum-classical dynamics. *Faraday Discuss.* **110**, 407. See <http://dx.doi.org/10.1039/A801824C>
- <sup>22</sup>Min SK, Agostini F, Gross EKV. 2015 Coupled-Trajectory Quantum-Classical Approach to Electronic Decoherence in Nonadiabatic Processes. *Phys. Rev. Lett.* **115**, 073001. See <http://dx.doi.org/10.1103/PhysRevLett.115.073001>
- <sup>23</sup>Meyer HD, Manthe U, Cederbaum LS. 1990 The Multi-Configurational Time-Dependent Hartree Approach. *Chem. Phys. Lett.* **165**, 73. See [http://dx.doi.org/10.1016/0009-2614\(90\)87014-I](http://dx.doi.org/10.1016/0009-2614(90)87014-I)

- <sup>24</sup>Meyer HD, Gatti F, Worth GA. 2009 *Multidimensional Quantum Dynamics: MCTDH Theory and Applications*. Weinheim: Wiley-VCH. See <https://www.wiley.com/en-us/Multidimensional+Quantum+Dynamics%3A+MCTDH+Theory+and+Applications-p-9783527627400>
- <sup>25</sup>Heller EJ. 1975 Time-dependent approach to semiclassical dynamics. *J. Chem. Phys.* **62**, 1544. See <http://dx.doi.org/10.1063/1.430620>
- <sup>26</sup>Heller EJ. 1981 Frozen Gaussians: A very simple semiclassical approximation. *J. Chem. Phys.* **75**, 2923. See <http://dx.doi.org/10.1063/1.442382>
- <sup>27</sup>Burghardt I, Meyer HD, Cederbaum LS. 1999 Approaches to the approximate treatment of complex molecular systems by the multiconfiguration time-dependent Hartree method. *J. Chem. Phys.* **111**, 2927. See <https://doi.org/10.1063/1.479574>
- <sup>28</sup>Ben-Nun M, Quenneville J, Martinez T. 2000 Ab Initio Multiple Spawning: Photochemistry from First Principles Quantum Molecular Dynamics. *J. Phys. Chem. A* **104**, 5161. See <http://dx.doi.org/10.1021/jp994174i>
- <sup>29</sup>Worth GA, Robb MA, Burghardt I. 2004 A novel algorithm for non-adiabatic direct dynamics using variational Gaussian wavepackets. *Faraday Discuss.* **127**, 307. See <http://dx.doi.org/10.1039/B314253A>
- <sup>30</sup>Saita K and Shalashilin DV. 2012 On-the-fly ab initio molecular dynamics with multiconfigurational Ehrenfest method. *J. Chem. Phys.* **137**, 22A506. See <http://dx.doi.org/10.1063/1.4734313>
- <sup>31</sup>Neville SP, Averbukh V, Patchkovskii S, Ruberti M, Yun R, Chergui M, Stolow A, Schuurman MS. 2016 Beyond structure: ultrafast X-ray absorption spectroscopy as a probe of non-adiabatic wavepacket dynamics. *Faraday Discuss.* **194**, 117. See <https://doi.org/10.1039/c6fd00117c>
- <sup>32</sup>Meek GA, Levine BG. 2016 The best of both Repts-Diabatized Gaussians on adiabatic surfaces. *J. Chem. Phys.* **145**, 184103. See <http://dx.doi.org/10.1063/1.4966967>
- <sup>33</sup>Joubert-Doriol L, Izmaylov AF. 2018 Nonadiabatic Quantum Dynamics with Frozen-Width Gaussians. *J. Phys. Chem. A* **122**, 6031. See <http://dx.doi.org/10.1021/acs.jpca.8b03404>
- <sup>34</sup>Mignolet B, Curchod BFE. 2018 A walk through the approximations of ab initio multiple spawning. *J. Chem. Phys.* **148**, 134110. See <https://doi.org/10.1063/1.5022877>

- <sup>35</sup>Makhov D V, Symonds C, Fernandez-Alberti S, Shalashilin DV. 2017 Ab initio quantum direct dynamics simulations of ultrafast photochemistry with Multiconfigurational Ehrenfest approach. *Chem. Phys.* **493**, 200. See <http://dx.doi.org/10.1016/j.chemphys.2017.04.003>
- <sup>36</sup>Richings GW, Polyak I, Spinlove KE, Worth GA, Burghardt I, Lasorne B. 2015 Quantum dynamics simulations using Gaussian wavepackets: the vMCG method. *Int. Rev. Phys. Chem.* **34**, 269. See <http://dx.doi.org/10.1080/0144235X.2015.1051354>
- <sup>37</sup>Xie C, Malbon CL, Yarkony DR, Guo H. 2017 Dynamic mapping of conical intersection seams: A general method for incorporating the geometric phase in adiabatic dynamics in polyatomic systems. *J. Chem. Phys.* **147**, 044109. See <https://doi.org/10.1063/1.4990002>
- <sup>38</sup>Meek GA, Levine BG. 2016 Wave function continuity and the diagonal Born-Oppenheimer correction at conical intersections *J. Chem. Phys.* **144**, 184109. See <http://dx.doi.org/10.1063/1.4948786>
- <sup>39</sup>Fedorov DA, Levine BG. 2019 A discontinuous basis enables numerically exact solution of the Schrödinger equation around conical intersections in the adiabatic representation. *J. Chem. Phys.* **150**, 054102. See <https://doi.org/10.1063/1.5058268>
- <sup>40</sup>Köppel H. 2004. *Diabatic Representation: Methods for the Construction of Diabatic Electronic States in Conical Intersections*, **15**, 175-204. Singapore: World Scientific. See [https://doi.org/10.1142/9789812565464\\_0004](https://doi.org/10.1142/9789812565464_0004)
- <sup>41</sup>Köppel H, Schubert B. 2006 The concept of regularized diabatic states for a general conical intersection. *Mol. Phys.* **104**, 1069. See <https://doi.org/10.1080/00268970500417937>
- <sup>42</sup>Richings GW, Worth GA. 2017 Multi-state non-adiabatic direct-dynamics on propagated diabatic potential energy surfaces. *Chem. Phys. Lett.* **683**, 606. See <https://doi.org/10.1016/j.cplett.2017.03.032>
- <sup>43</sup>Fernandez-Alberti S, Makhov DV, Tretiak S, Shalashilin DV. 2016 Non-adiabatic excited state molecular dynamics of phenylene ethynylene dendrimer using a multiconfigurational Ehrenfest approach. *Phys. Chem. Chem. Phys.* **18**, 10028. See <http://dx.doi.org/10.1039/C5CP07332D>
- <sup>44</sup>Joubert-Doriol L, Sivasubramanium J, Ryabinkin IG, Izmaylov AF. 2017 Topologically correct quantum nonadiabatic formalism for on-the-fly dynamics. *J. Phys. Chem. Lett.* **8**, 452. See <http://dx.doi.org/10.1021/acs.jpcllett.6b02660>
- <sup>45</sup>Joubert-Doriol L, Izmaylov AF. 2018 Variational nonadiabatic dynamics in the moving crude adiabatic representation: Further merging of nuclear dynamics and electronic struc-

- ture. *J. Chem. Phys.* **148**, 114102. See <https://doi.org/10.1063/1.5020655>
- <sup>46</sup>Curchod BFE. 2020 *Full and Ab Initio Multiple Spawning in Quantum Chemistry and Dynamics of Excited States*. John Wiley & Sons, Ltd, 435-467. See <http://dx.doi.org/10.1002/9781119417774.ch14>
- <sup>47</sup>Ibele LM, Nicolson A, Curchod BFE. 2020 Excited-state dynamics of molecules with classically driven trajectories and Gaussians. *Mol. Phys.* **118**, 8. See <https://doi.org/10.1080/00268976.2019.1665199>
- <sup>48</sup>Cederbaum LS. 2004. *Born-Oppenheimer Approximation and Beyond in Conical Intersections*, **15**, 3-40. Singapore: World Scientific. See [https://doi.org/10.1142/9789812565464\\_0001](https://doi.org/10.1142/9789812565464_0001)
- <sup>49</sup>Cattarius C, Worth GA, Meyer HD, Cederbaum LS. 2001 All mode dynamics at the conical intersection of an octa-atomic molecule: Multi-configuration time-dependent Hartree (MCTDH) investigation on the butatriene cation. *J. Chem. Phys.* **115**, 2088. See <http://dx.doi.org/10.1063/1.1384872>
- <sup>50</sup>Izmaylov AF, Mendive-Tapia D, Bearpark MJ, Robb MA, Tully JC, Frisch MJ. 2011 Nonequilibrium Fermi golden rule for electronic transitions through conical intersections. *J. Chem. Phys.* **135**, 234106. See <http://dx.doi.org/10.1063/1.3667203>
- <sup>51</sup>Maskri R, Joubert-Doriol L. XXXX Supplementary information for “The moving crude adiabatic alternative to the adiabatic representation in excited state dynamics”.
- <sup>52</sup>Eaton JW, Bateman D, Hauberg S, Wehbring R. 2017 GNU Octave version 4.2.1 manual: a high-level interactive language for numerical computations. See <https://www.gnu.org/software/octave/doc/v4.2.1/>